INTERFACE

rsif.royalsocietypublishing.org

Research

Cite this article: Xiao M, Chen W, Li W, Zhao J, Hong Y-lee, Nishiyama Y, Miyoshi T, Shawkey MD, Dhinojwala A. 2018 Elucidation of the hierarchical structure of natural eumelanins. *J. R. Soc. Interface* **15**: 20180045.
http://dx.doi.org/10.1098/rsif.2018.0045

Received: 17 January 2018
Accepted: 13 February 2018

Subject Category:
Life Sciences–Chemistry interface

Subject Areas:
biochemistry, evolution, biophysics

Keywords:
melanin, eumelanin, hierarchical structure

Authors for correspondence:
Toshikazu Miyoshi
e-mail: miyoshi@uakron.edu
Matthew D. Shawkey
e-mail: matthew.shawkey@ugent.be
Ali Dhinojwala
e-mail: ali4@uakron.edu

†These authors contributed equally to this study.

Electronic supplementary material is available online at https://dx.doi.org/10.6084/m9.figshare.c.4010347.

THE ROYAL SOCIETY PUBLISHING

Elucidation of the hierarchical structure of natural eumelanins

Ming Xiao[1,†], Wei Chen[2,†], Weiyao Li[1], Jiuzhou Zhao[1], You-lee Hong[1,3], Yusuke Nishiyama[3,4], Toshikazu Miyoshi[1], Matthew D. Shawkey[5] and Ali Dhinojwala[1]

[1]Department of Polymer Science, The University of Akron, Akron, OH 44325, USA
[2]State Key Lab of Pollution Control and Resource Reuse Study, College of Environmental Science and Engineering, Tongji University, Shanghai 200092, People's Republic of China
[3]RIKEN CLST-JEOL Collaboration Center, RIKEN, Yokohama 230-0045, Japan
[4]JEOL RESONANCE Inc., Tokyo 196-8558, Japan
[5]Evolution and Optics of Nanostructures Group, Department of Biology, University of Ghent, Ghent 9000, Belgium

MX, 0000-0003-2354-2059; MDS, 0000-0002-5131-8209; AD, 0000-0002-3935-7467

Eumelanin is one of the most ubiquitous pigments in living organisms and plays an important role in coloration and UV protection. Because eumelanin is highly cross-linked and insoluble in solvents, the chemical structure is still not completely known. In this study, we used atomic force microscopy, X-ray photoelectron spectroscopy and solid-state nuclear magnetic resonance (NMR) to compare intact eumelanosomes (pigment granules mostly made of eumelanin) from four phylogentically distant species: cuttlefish (*Sepia officinalis*) inks, black fish crow (*Corvus ossifragus*) feathers, iridescent wild turkey (*Melleagris gallopavo*) feathers and black human hair. We found that eumelanosomes from all four species are composed of subunit nanoparticles with a length of 10–60 nm, consistent with earlier observations in eumelanosomes from the sepia ink and human hair. The solid-state NMR results indicate the presence of quinone methide tautomers in all four eumelanins. We also found clear differences in the UV absorbance, the ratio of 5,6-dihydroxyindole-2-carboxylic acid/5,6-dihydroxyindole and protonated aryl carbon ratios in sepia eumelanin relative to the other three. This comparison of natural eumelanin across a phylogenetically broad group of organisms provides insights into the change in the eumelanin structure over the evolutionary history and enables the production of synthetic eumelanin with properties that are similar to natural eumelanin.

1. Introduction

Eumelanin is a major melanin pigment type found in bacteria, fungi, plants, animals and extinct organisms, and plays a significant role in ultraviolet (UV) protection, detoxification, metal binding and structural coloration [1–5]. Furthermore, *in vitro* studies have shown that eumelanin has unique physicochemical properties, including broadband light absorption [6], intrinsic-free radical quenching [7], efficient non-radiative energy transfer [8] and humidity-dependent electronic semiconductivity [9]. Recently, researchers have investigated eumelanin-like materials for applications in the areas of catalysts [10], biomedical science [11–14], energy storage [15,16], nanocomposites [17–19] and structural coloration [20–23].

Eumelanin is biosynthesized from tyrosine in specialized cells called melanocytes. This process involves a series of enzyme-catalysed reactions in which eumelanin precursors—5,6-dihydroxyindole (DHI), 5,6-dihydroxyindole-2-carboxylic acid (DHICA) and their oxidized forms—are cross-linked into eumelanin through chemical bonds or physical interactions (figure 1) [24]. X-ray diffraction and high-resolution transmission electron microscopy show planar eumelanin protomolecules (oligomers of DHI and DHICA) of 13–20 Å

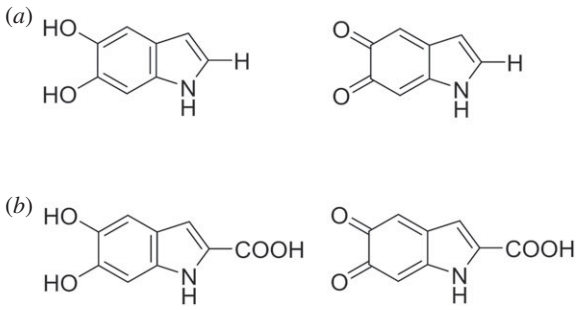

Figure 1. Eumelanin's main precursors. (*a*) DHI and its oxidized form. (*b*) DHICA and its oxidized form.

in length that are stacked into lamellae with a spacing of 3.7–4.0 Å [25,26]. However, the exact chemical structure of eumelanin remains elusive, mainly due to its insolubility in solvents, close binding with other cellular tissues and an amorphous structure [27]. These challenges have led researchers to study synthetic melanins, using experimental techniques such as Fourier transform (FT)-IR [28], X-ray photoelectron spectroscopy (XPS) [29], mass spectroscopy [30] and solid-state nuclear magnetic resonance (NMR) [28,31,32], as well as theoretical simulations [33–36]. However, the chemical structures of synthetic eumelanin are highly dependent on the monomer type (dopamine, L-DOPA and tyrosine) and reaction conditions (temperature, pH, oxidants and reaction time) during the synthesis [37–40]. Since it is not ideal to use synthetic eumelanin to infer the structure of natural eumelanin, there is a need to directly investigate the structure of natural eumelanin.

Most studies of natural eumelanin have focused on eumelanin from the cuttlefish (*Sepia officinalis*) ink [3,25,41] and occasionally eumelanin from human hair, retinas or fungi [42,43]. Only a few studies have investigated the structure of intact natural eumelanosomes (without chemical degradation) from phylogenetically distant species [44]. Here, we used multiple non-destructive techniques to compare the structure of eumelanins extracted from cuttlefish (*S. officinalis*) ink, feathers of two avian species (black fish crow *Corvus ossifragus* and iridescent wild turkey *Melleagris gallopavo* feathers) and black hair from humans. We characterized their morphologies using atomic force microscopy (AFM), elemental compositions with XPS and chemical structure using multiple solid-state NMR techniques. This intensive characterization of natural eumelanin from a phylogenetically broad group of organisms is of fundamental interest and may enable a more precise design of synthetic eumelanin for diverse applications.

2. Experimental section

2.1. Eumelanin preparation

We extracted natural eumelanosomes from crow wing feathers, iridescent turkey wing feathers and black human hair, following a reported protocol with some modifications [45]. Those feathers and hair were obtained from several individuals and therefore extracted eumelanosomes represented the average composition of those species. Feathers/hair (approx. 2 g) were washed using acetone three times and deionized (DI) water once, and then cut into small pieces. We added the pieces to 40 ml of 0.1 M phosphate buffer (pH 7.5) with 0.4 g of dithiothreitol (DTT, Fisher Scientific). The mixture was degassed under N_2 and then shaken at 37°C overnight. We added 1 ml of proteinase-K (20 mg ml^{-1}, Amresco) and 0.2 g of DTT to the suspension and continued to shake the mixture for 24 h. Next, the black suspension was centrifuged at 4000*g* and rinsed with DI water six times. The precipitate was suspended in 16 ml of phosphate buffer with 16 mg of papain (ACROS organics) and 80 mg of DTT overnight. After 24 h, the suspension was centrifuged at 4000 *g* and washed using DI water six times. The precipitate was suspended in 16 ml of phosphate buffer with 0.4 ml of proteinase-K and 32 mg of DTT overnight. Then, centrifugation was done to remove supernatant and 6 ml of degassed phosphate buffer with 0.12 ml of Triton X-100 (Sigma Aldrich) was added. Triton X-100 served as a surfactant to break the lipid membranes of eumelanosomes. The new suspension was shaken for 4 h and washed using methanol three times, then water three times. The precipitate was dispersed in 16 ml of phosphate buffer solution with 0.4 ml of proteinase-K and 32 mg of DTT, and the mixture was shaken overnight at 37°C. Finally, we suspended the precipitate in 8 ml of phosphate buffer with 0.2 ml of proteinase-K and 16 mg of DTT and stirred the mixture at 37°C overnight. All the enzyme-catalysed reactions were done in the incubator at 37°C. Next, we washed the eumelanosomes using DI water three times. The sample was dried and weighed to be about 100 mg. Sepia eumelanin in the form of melanin granules (referred to here as eumelanosomes for simplicity) was purchased from Sigma Aldrich without any treatment. As a control, synthetic eumelanin nanoparticles were prepared by oxidation and polymerization of dopamine in a mixture of water, ethanol and ammonia according to our previously published protocol [46].

2.2. Morphological characterization

Extracted eumelanosomes were placed onto aluminium stubs using a double-sided carbon black tape and imaged using a field emission scanning electron microscope (SEM) (JEOL-7401, JEOL Ltd). We measured the sizes of 50 eumelanosomes for each species using ImageJ. We also dispersed eumelanosomes into water to make a dilute solution and placed a small droplet onto carbon-coated copper grids. After complete evaporation of water, we used a transmission electron microscope (TEM) (JEM-1230, JEOL Ltd.) to image the eumelanosome morphology. For AFM measurements, dilute eumelanosome solutions were drop-casted onto clean silicon wafers and the deposits were characterized using a Dimension ICON AFM machine (Bruker) in the tapping mode and a scan rate of 0.6 Hz. We used a silicon tip with radius <10 nm, spring constant 7.8 N m^{-1} and resonant frequency 150 kHz (ACSTA, Applied NanoStructures, Inc.). The cantilever had an aluminium reflective coating on the back side.

2.3. Spectroscopy characterization

XPS measurements were performed on extracted eumelalnins using the PHI 5000 instrument with Al Kα radiation as an excitation source (100 µm, 15 kV, 25 W). We used a base pressure less than 2×10^{-8} Pa and operating pressure of approximately 2×10^{-6} Pa. The 117.4 eV pass energy was used for survey scans (0–1400 eV, two scans) and pass energy of 11.75 eV was used for the high-resolution C1s scans (278–292 eV). We reported here the average results

from three scans. Ar^+ ion beam was used for surface charge neutralization. We used the Multipak software to fit the high-resolution C1s spectra.

To measure the FT-IR spectra, we first ground the eumelanin powders and potassium bromide (FT-IR grade, Sigma Aldrich) and then compressed the sample to a semi-transparent pellet (approx. 0.5 mm thick). The FT-IR measurements were done at room temperature and relative humidity of 57–58%. The IR absorbance of the sample pellets was measured from 1000 to 4000 cm^{-1} using a FT-IR machine (Nicolet iS50, Thermal Scientific).

For the UV–vis absorption measurements, we used dilute solutions of melanosomes in water (20 mg l^{-1}) and used a probe sonicator Q125 (125 W, Qsonica LLC) to break down the aggregates of melanosomes. The sizes of melanosomes were measured using dynamic light scattering (a BI-HV Brookhaven Instrument with a 633 nm solid-state laser). The UV–vis absorption spectra of four eumelanosome solutions were obtained using a Cary 100 Bio UV–visible spectrophotometer (Agilent Technologies). The dilute solution was necessary to reduce the scattering of light. To examine if the absorbance is mainly caused by absorbance rather than scattering, we also measured the absorption of aqueous solutions of silica particles at the same concentration (silica particle diameter, 1 μm).

2.4. Solid-state NMR measurements

For the ^{13}C CP/MAS and heteronuclear correlation (HETCOR) NMR experiments, we used a Bruker Avance 300 MHz NMR machine with resonance frequencies of 300.3 MHz for ^1H and 75.5 MHz for ^{13}C. A 4 mm double-resonance probe at a magic angle spin (MAS) frequency of 12 kHz was used to suppress the spinning side band. The ^{13}C and ^1H chemical shifts were calibrated externally based on the methine peak of adamantane at 29.46 ppm and the single peak of tetramethylsilane at 0 ppm, respectively. For the ^{13}C CP/MAS spectra, a 4 μs pulse length was used for the $\pi/2$ pulse for both ^1H and ^{13}C channels, corresponding to radio frequency (RF) field strength of 62.5 kHz. The ^1H–^{13}C cross-polarization (CP) contact time and relaxation delay (RD) time were set to 2 ms and 2 s, respectively. A ^1H two-phase pulse modulation (TPPM) with a $\pi/2$ pulse length of 4 μs was applied during the ^{13}C signal acquisition. To compare the non-protonated aryl carbons in four eumelanins, we performed the spin-echo and dipolar-dephasing experiments with a recoupled dipolar interaction at MAS frequency of 12 kHz [47,48]. We used the Bruker top-spin software to integrate the peak areas and calculated the noise-to-signal ratio to calculate the measurement errors. For the HETCOR measurements, the RF strength of ^1H channel was set to 80.65 kHz, and a 100 μs contact time was used in the CP experiments to suppress the long-range spin diffusion effect. The RD time was set to 2s. For the ^1H channel, Lee-Goldburg (FSLG) field with strength of 98.63 kHz was used to suppress the homo-nuclear coupling. The TPPM decoupling with strength of 80.65 kHz was used during the acquisition process. A total of 256 points in t_1 dimension with a total number of 1024 scans were executed to acquire the complete spectrum. Glycine was used as an external standard material to calibrate the chemical shifts in the ^1H spectra.

To obtain ^1H single quantum (SQ)–double quantum (DQ) correlation spectra, we used a JNM-ECZ900R spectrometer (JEOL RESONANCE, Inc., Japan) at 21.1 T with resonance frequencies of 900 and 226.5 MHz for ^1H and ^{13}C, respectively. For this instrument, we used a 0.75 mm triple-resonance MAS probe with a MAS rate of 80 kHz. The ^1H–^1H dipolar couplings were achieved by a back-to-back (BABA) pulse sequence [49]. Approximately 0.3 mg of sample was loaded into a 0.75 mm MAS rotor. The RF field strength of ^1H nuclei was 440.5 kHz at the $\pi/2$ pulse length of 0.6 μs. We collected data using a RD time of 2 s and we averaged 32 scans. The excitation time and reconversion periods were set to 90.4 μs. All spectra were measured in 32 rows with $\Delta t_1 = 25$ μs, and thus, the total acquisition time was approximately 2 h. The experimental conditions were optimized by observing the NMR spectra of U-^{13}C/^{15}N-L-alanine. The ^1H chemical shift frequency was referenced externally to ^1H, a methine resonance of L-alanine at 3.78 ppm. The spectra were processed using the Delta software (JEOL RESONANCE, Inc.).

3. Results and discussion

3.1. Morphology of eumelanosomes

Eumelanosomes extracted from sepia inks, crow wing feathers, wild turkey tail feathers and human hair have distinct shapes and sizes (figure 2*a–d*). Our enzymatic extraction successfully removed the keratin matrix, because sheets of keratin fibres can be seen if the extraction is not complete (electronic supplementary material, figure S1), and these are not observed in our final samples. Sepia eumelanosomes are aggregates of spherical nanoparticles with diameters of 123 ± 28 nm. The other three eumelanosomes (extracted from crow, turkey feathers and human hair) are well-defined rod-shaped particles with a length of 890–1570 nm and a diameter of 234–307 nm (figure 2*e*). Turkey eumelanosomes are hollow, while the other three are solid (figure 2*a–d*). We have recently shown evidence that hollow turkey eumelanosome form via a different melanogenesis process from solid ones [23] and the different shapes of eumelanosomes are likely controlled by genetic factors in different species [50]. Interestingly, all eumelanosomes with different morphologies contain 10–60 nm secondary nanoparticles (figure 3), consistent with previous work showing similar subunit small nanoparticles in sepia and human melanosomes [51]. High-resolution TEM images show rough surfaces for all four samples (electronic supplementary material, figure S2). This similarity between differently shaped eumelanosomes from diverse species likely suggests that secondary nanoparticles form first and then assemble into sub-micron eumelanosome with different morphologies.

3.2. Chemical structural analysis

Eumelanin is insoluble in almost all solvents, and in any case, it is desirable to perform the structural analysis in the solid state to keep them intact without any degradation. First, we used XPS survey scans to obtain the elemental compositions of eumelanin, where elements below 0.5% were considered as noise. Four natural eumelanins mainly contained carbon (66.3–67.4%), oxygen (18.8–22.2%) and nitrogen (8.7–12.9%) (electronic supplementary material, table S1). Previous work showed that the high-resolution C1s XPS provided the most useful information on the chemical structure of synthetic eumelanin [29,41], and, thus, we

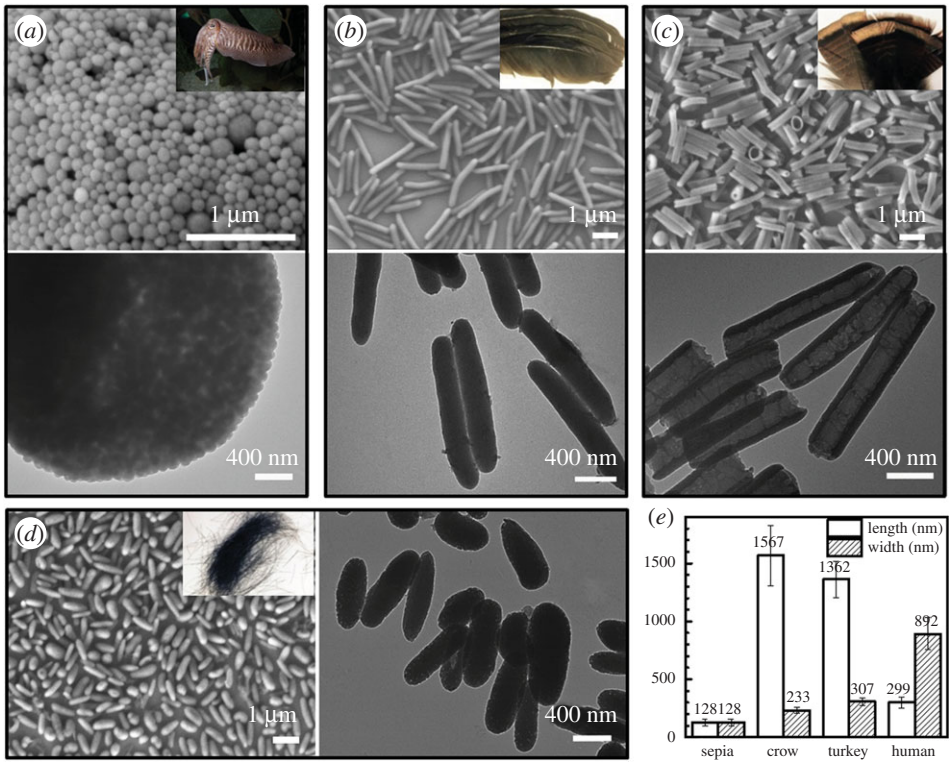

Figure 2. SEM and TEM images of eumelanosomes extracted from (*a*) sepia ink, (*b*) crow feathers, (*c*) turkey feathers and (*d*) human hair. Insets are photos of cuttlefish (credit Brian Gratwicke), crow feathers, turkey feathers and human hair. (*e*) Sizes of four types of eumelanosomes. (Online version in colour.)

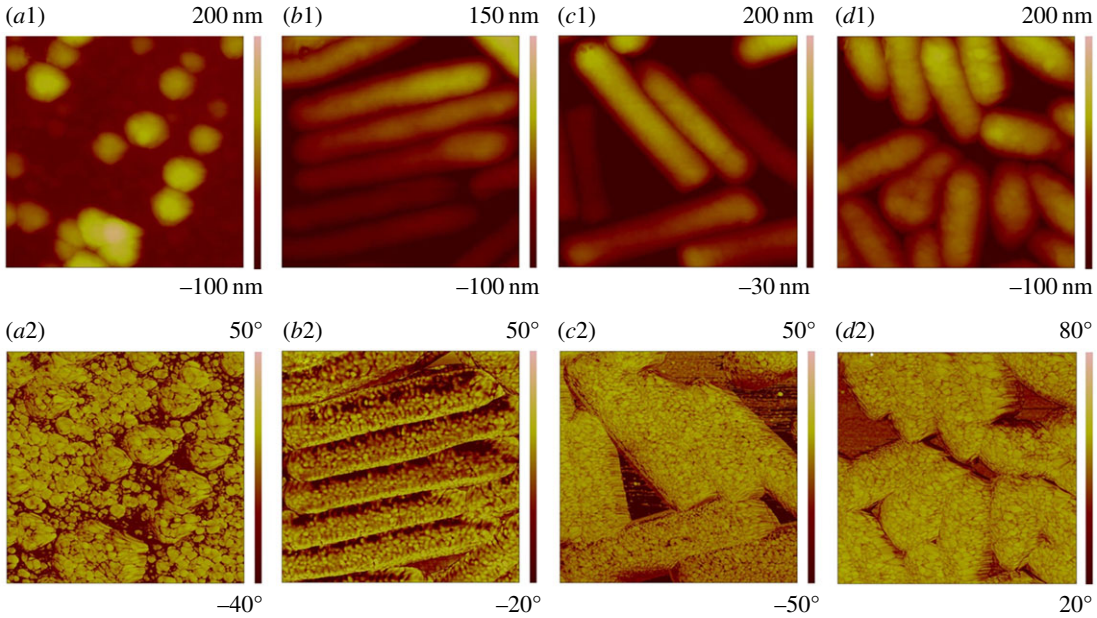

Figure 3. AFM height and phase images of (*a*1,*a*2) sepia, (*b*1,*b*2) crow, (*c*1,*c*2) turkey and (*d*1,*d*2) human eumelanosomes. Sizes of all images are 2 × 2 µm.

focused on high-resolution spectra of C1s here. After obtaining the raw data of C1s scans, we corrected the whole spectra by shifting the largest peak to 285 eV and performed peak fitting using five peaks according to the literature: C–C(H) at approximately 284.9 ± 0.2 eV, C–OH/C–N at approximately 286.3 ± 0.2 eV, C=O at approximately 288.1 ± 0.2 eV, O–C=O at approximately 289.3 ± 0.2 eV and a $\pi \rightarrow \pi^*$ shake-up peak at 290–292 eV (electronic supplementary material, figure S3) [29,41]. All four eumelanins have similar concentrations of functional groups of C–C(H) and C–OH/C–N, but different percentages of C=O and O–C=O (figure 4). The ratio between C=O and O–C=O is 7.0 ± 0.2 for sepia, 1.9 ± 0.1 for crow, 3.6 ± 0.1 for turkey and 1.4 ± 0.1 for human eumelanosome. Because natural eumelanin likely consists primarily of DHI, DHICA and their oxidized forms (figure 1) [52], their amount of O–C=O group should represent the concentration of DHICA-type monomer (DHICA and its oxidized form). Therefore, sepia eumelanin is likely to contain the least DHICA-type monomer and human has the most DHICA-type monomer. In addition,

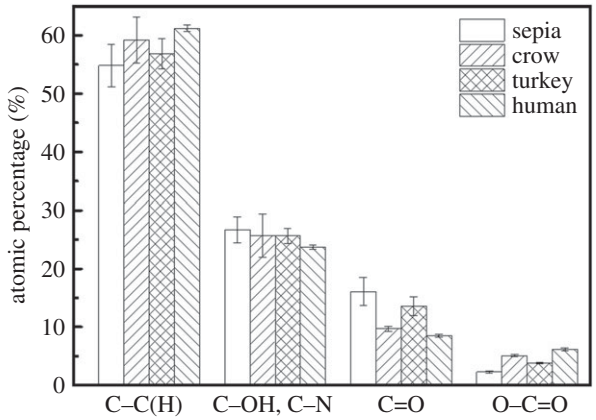

Figure 4. Relative percentages (%) of carbon bonding measured using high-resolution XPS spectra of C1s for four different natural eumelanins.

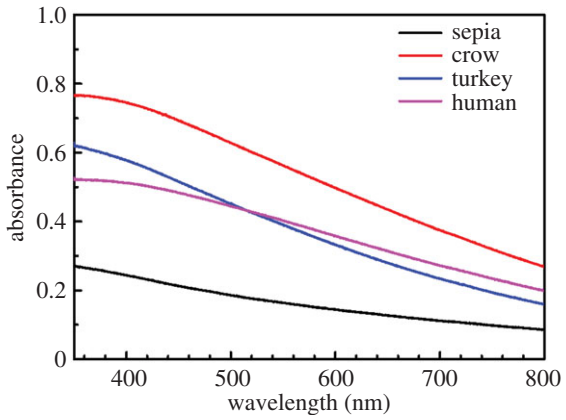

Figure 5. UV–vis absorbance spectra of four natural eumelanins in aqueous solutions (25 mg l^{-1}).

sepia and turkey eumelanin contain more C= O than the other two types of eumelanin possibly due to relatively higher concentration of quinone structures (oxidized DHI/DHICA).

Research on synthetic eumelanin has revealed that the DHICA component in the eumelanin contributes more to absorption of light and UV protection than the DHI component [39,53]. These findings suggest that it is critical to quantify the ratios of DHICA and DHI components in the eumelanin. The most common way to do so is to examine degradation products of the eumelanin after a strong oxidation reaction with $KMnO_4$. DHI components turn into pyrrole-2,3-dicarboxylic acid (PDCA), while DHICA components change to pyrrole-2,3,5-tricarboxylic acid (PTCA). However, this method ignores the possibility that chemically cross-linked DHI components may also become PTCA after strong oxidation, reducing the accuracy of this method. The use of XPS provides a facile, non-destructive method to distinguish the ratio between DHICA and DHI, even though it mostly probes the top 10 nm layer thickness.

All four types of eumelanin have broadband absorption of light ranging from 350 to 800 nm (figure 5). A solution of silica microparticles (approx. 1 µm, larger than all eumelanosomes, electronic supplementary material, figure S4) shows much smaller absorbance than eumelanin (electronic supplementary material, figure S5). Silica has negligible absorption across 350–800 nm and its measured absorbance is caused by scattering [54]; therefore, the scattering effect is much smaller than absorption in eumelanin UV–vis spectra and the spectra in figure 5 are a good approximation of eumelanin's true absorption. The absorbance of sepia eumelanin is much less than that of bird and human eumelanins, seemingly consistent with the argument that DHICA component absorbs more light than the DHI component. However, crow eumelanin has a higher absorption but a smaller DHICA component than human eumelanin. Therefore, contrary to previous suggestions [53], the DHICA content does not seem to have a simple positive correlation with UV absorption.

The chemical structures of eumelanin were further investigated using FT-IR. The four eumelanins have similar broad peaks near 3300, 1620 and 1360 cm^{-1} (electronic supplementary material, figure S6) in FT-IR spectra. The 3300 cm^{-1} peak originates from O–H and N–H stretching vibrations. The 1620 cm^{-1} is probably caused by a combination of C= O stretching of the carbonate group and/or C= C aromatic ring vibration. The 1360 cm^{-1} peak is from the indole ring vibration and/or C–N stretching [55,56]. The FT-IR spectrum of sepia eumelanin shows a weaker 3300 cm^{-1} peak in comparison to the other three eumelanins, probably due to less O–H, consistent with the XPS data that sepia contained more quinone structures. It is still challenging to further quantify the differences and/or similarities in the chemical structure based on FT-IR spectra due to the broad overlapping peaks.

3.3. Solid-state NMR

Quantification of the protonated aryl carbons in natural eumelanin is critical to revealing their chemical structure, because this percentage is directly related to the DHICA/DHI monomer ratio and their cross-linking density in the eumelanin. More importantly, this percentage governs the macroscopic properties such as UV protection and detoxification [39,53]. As shown in figure 1, the DHICA-type monomer (three protonated out of eight aryl carbons) has fewer protonated aryl carbons than the DHI-type monomer (four protonated out of eight aryl carbons). In addition, a higher degree of cross-linking leads to a lower percentage of protonated aryl carbons. To quantify the protonated aryl carbons among four eumelanins, we measured and compared the ^{13}C spin-echo and dipolar-dephasing CP/MAS NMR spectra. ^{13}C spin-echo CP/MAS NMR spectra display all kinds of carbon species, whereas ^{13}C dipolar-dephasing CP/MAS spectra only present non-protonated carbons (except for methyl carbons with ultrafast dynamics at ambient temperature) (figure 6) [47,48]. The broadening of the spectra is likely caused by the intrinsic properties of the eumelanin, which can also be observed in both natural and synthetic eumelanin in other studies [28,31,57,58]. The ^{13}C CP/MAS technique could not offer quantitative results as precisely as ^{13}C DP/MAS due to differences in the CP efficiency of different nuclei. However, limited by the low sensitivity of eumelanin samples (one ^{13}C CP/MAS spectrum with acceptable signal-to-noise ratio took at least 12 h), collection of a ^{13}C DP/MAS spectrum with a much longer RD time for eumelanin is almost impossible. Meanwhile, ^{13}C CP/MAS has been used to do quantitative analysis in complicated systems, such as semi-crystalline polymers [59]. Our following results are calculated based on the assumption that all ^{13}C nuclei have the same CP efficiency in the aromatic region (100–160 ppm).

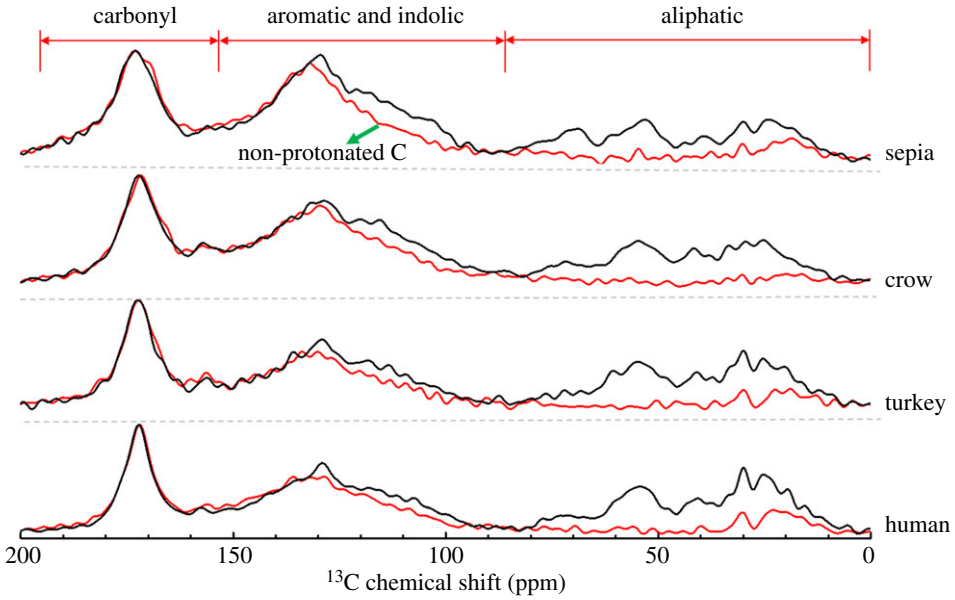

Figure 6. ^{13}C CP/MAS NMR spectra of spin-echo (black curves) and dipolar-dephasing (red curves) measurements on four eumelanins.

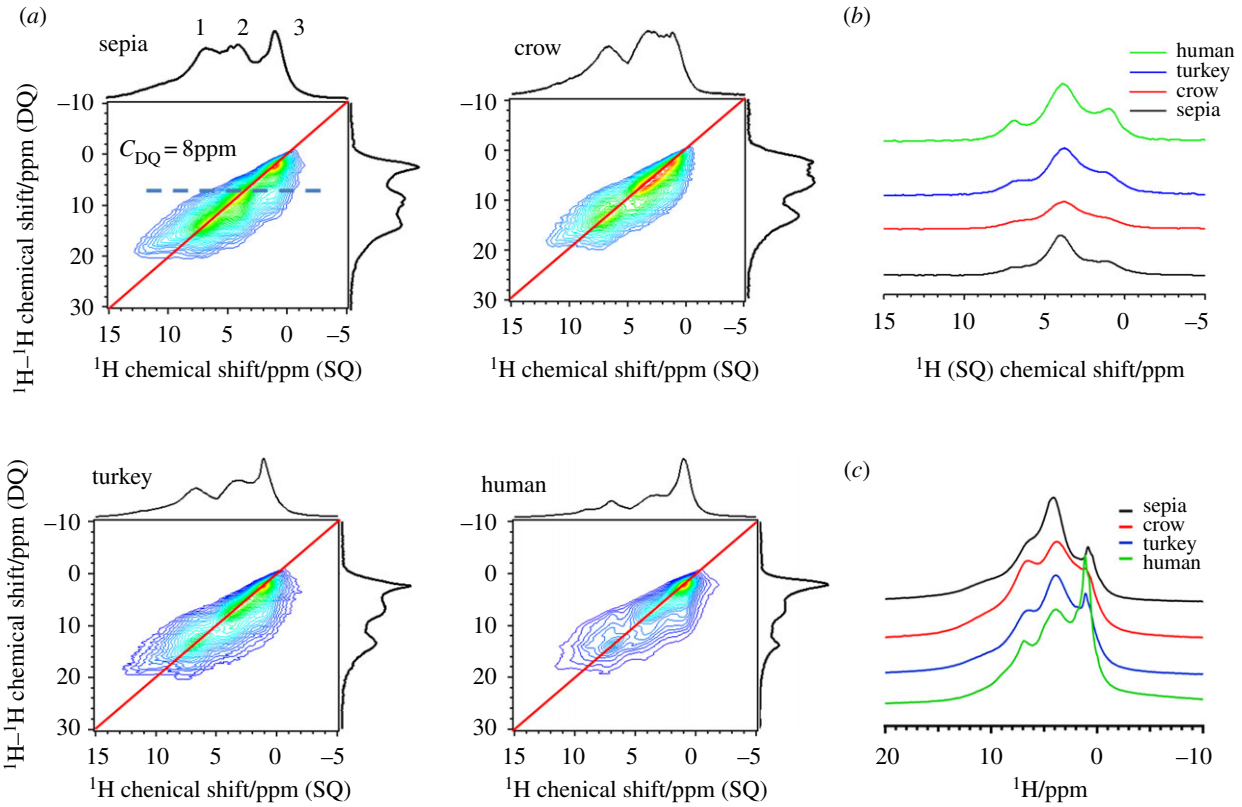

Figure 7. (*a*) Two-dimensional contour plots of ^{1}H SQ–DQ NMR spectra of sepia, crow, turkey and human eumelanins. (*b*) One-dimensional ^{1}H spectra obtained from slicing two-dimensional spectra at C_{DQ} = 8 ppm as marked by the dot line in sepia SQ–DQ NMR spectrum. (*c*) Solid-state ^{1}H NMR (ν_r = 50 kHz) spectra of four eumelanins.

In ^{13}C spin-echo CP/MAS NMR spectra, the peak at approximately 172 ppm is assigned to carbonyl groups from the DHICA component and quinone structure in eumelanin [6,52]. All eumelanins show a broad peak at approximately 130 ppm spanning from 100 to 160 ppm, which originates from both protonated and non-protonated aromatic carbons in different chemical environments. We normalized the spectra of spin-echo and dipolar-dephasing NMR based on carbonyl peaks (approx. 172 ppm) and calculated the ratio of the aromatic peak area (100–160 ppm) between dipolar-dephasing and spin-echo experiments. This ratio of area indicates the percentage of non-protonated aryl carbons in the eumelanin, and we can thus obtain the protonated aryl carbon percentages for all eumelanosomes. The sepia eumelanin contains the highest percentage of protonated aryl carbons (17.7 ± 0.5%), crow and turkey have comparable amounts (14.1 ± 0.3% and 15.5 ± 0.5%) and human eumelanin has the lowest percentage (12.1 ± 0.5%).

We can combine the protonated aryl carbon percentages from NMR and DHICA compositions from the XPS data to

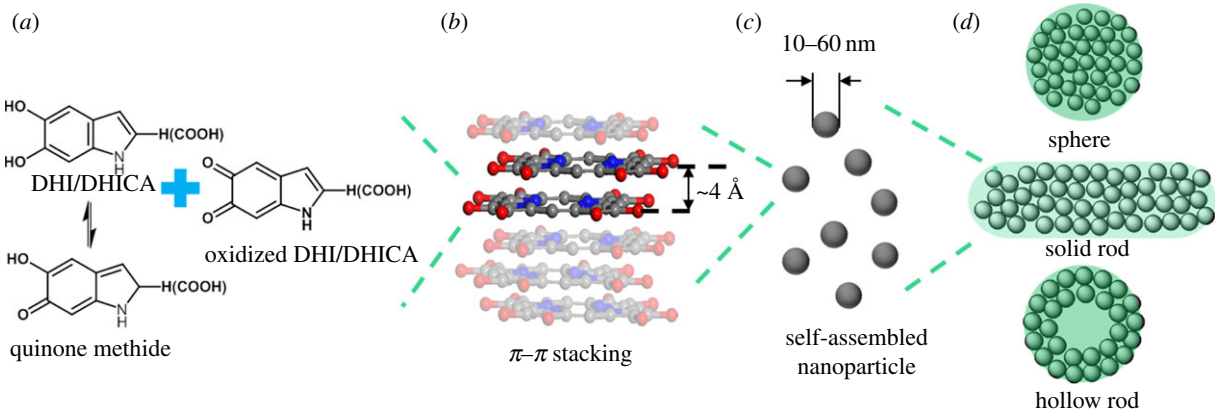

Figure 8. A proposed hierarchical structure for natural eumelanin. (*a*) Eumelanin monomers, (*b*) $\pi-\pi$ stacking of eumelanin blocks, (*c*) subunit nanoparticles and (*d*) eumelanosomes with different morphologies.

estimate the cross-linking density to be approximately 63–72%, based on an assumption that eumelanin is only composed of DHI and DHICA monomers (see electronic supplementary material for more details). Although this estimation is based on the assumption that the natural eumelanin is only made of two starting monomers, it provides an estimate of the cross-linking density of eumelanin.

To understand the intermolecular interactions of natural eumelanin, we used high-resolution two-dimensional ^{1}H SQ–DQ correlation to detect the inter-nuclear correlation among protons. Two-dimensional ^{1}H SQ–DQ has been widely used to extract intermolecular information [60]. Generally, if two spins (a and b ppm) interact with each other, a signal with a NMR resonance line of (a + b) ppm can be observed in the F1 (DQ) dimension. For all four eumelanins, three distinct ^{1}H resonances located at 6.5 ppm (peak 1, aryl protons), 4.0 ppm (peak 2, unclear) and 1.0 ppm (peak 3, aliphatic protons) were observed with different intensities in two-dimensional ^{1}H DQ spectra (figure 7*a*).

All spectra of the four eumelanins show strong diagonal peaks representing strong spatial correlations of the same type of protons (figure 7*a*). Dipolar-dephasing CP/MAS data in figure 6 show a low percentage of protonated aryl carbons (12–18%) in four types of eumelanins, and we can estimate the average of 0.96–1.44 protons per monomer based on the information that both DHI- and DHICA-type monomers contain eight aryl carbons. Strong diagonal peaks from peak 1 in the aromatic region mainly originate from the intermolecular interactions. Meanwhile, the cross-peak between protons from peaks 1 and 3 is not observed. The absence of the off-diagonal peaks suggests a microphase separation of aromatic and aliphatic domains. The $\pi-\pi$ stacking and the repulsion force between the rigid aromatic and the flexible aliphatic functional groups are common driving forces in nature and have been used to design well-defined supramolecular architecture, like triphenylene [61] and hexa-peri-hexabenzocoronene derivatives [62]. Therefore, we hypothesize that these intermolecular interactions of aromatic protons are caused by $\pi-\pi$ stacking (figure 8), in agreement with some other studies on natural and synthetic eumelanin [25,26].

We used two-dimensional HETCOR NMR spectra to determine the peak assignments of protons from peak 2, which were not clear from the proton NMR spectra. The HETCOR technique correlates ^{1}H and ^{13}C directly, and such correlation leads to a cross-peak in the two-dimensional spectra. Here, we set the CP contact time as low as 100 µs to suppress the long-range ^{1}H–^{13}C (2.6–3.0 Å) cross-polarization and primarily detect the proximity of certain protons [63]. The typical inter-nuclear distance of ^{1}H–^{13}C covalent bond is 1.07–1.09 Å [64]. The HETCOR peak volume is proportional to $1/r^{3}$ when the CP contact time is short [65]. Therefore, our HETCOR spectra contain quite minor signals (less than 2%) from the intermolecular magnetization transfer, such as $\pi-\pi$ stacking with an intermolecular distance of approximately 4 Å as proposed in eumelanin [34,35]. As a result, two-dimensional ^{1}H–^{13}C HETCOR results with a short contact time probe protonated carbon, including aryl and alkyl carbons as shown in electronic supplementary material, figure S7. Protons from peak 2 are directly correlated with ^{13}C with chemical shift of 60–40 ppm, which most likely come from saturated carbons. Inspired by the previous simulation work showing that the quinone methide is the most stabilized tautomer of DHI [66], we believe that the peak 2 comes from quinone methides in the eumelanin (figure 8*a*). In addition, the spatial distribution of protons from peak 2 is observed through ^{1}H SQ–DQ spectrum through the slice data $C_{DQ} = 8$ ppm as shown in figure 7*b*. Protons from peak 2 display a stronger interaction with aromatic (peak 1) and aliphatic protons (peak 3) in human eumelanin when compared with other three eumelanins, likely due to a higher number of protons from peak 3 in the human eumelanin (figure 7*c*). The influence of such differences among four eumelanins on macroscopic performance requires further investigation.

3.4. Synthetic eumelanin

We used the most common synthetic eumelanin, polydopamine, as a control to help understand natural eumelanin structure and properties. Synthetic eumelanin particles also contain subunit nanoparticles and broadly absorb UV–visible light (electronic supplementary material, figures S8 and S9), similar to natural eumelanin. However, its chemical structure is quite different from natural eumelanin based on FT-IR and solid-state NMR spectra. FT-IR spectrum of synthetic eumelanin shows two extra distinct peaks at 1512 and 1289 cm^{-1} (electronic supplementary material, figure S6). In the solid-state NMR spectra, synthetic eumelanin has much smaller resonance at the carbonyl region, and the

aromatic region has two extra peaks at approximately 118 ppm and approximately 145 ppm, in addition to the 130 ppm peaks shared by all natural eumelanins (electronic supplementary material, figure S10). Therefore, so-called synthetic eumelanin (at least polydopamine) differs chemically from natural eumelanin and our efforts to elucidate the structures of natural eumelanin are critical to the design of more realistic synthetic eumelanin.

4. Conclusion

We have compared the morphology and chemical structure of eumelanins from four phylogenetically distant species using multiple non-destructive characterization tools. We propose a common hierarchical structure for natural eumelanins (figure 8), in which most variations between species occur at the molecular level, particularly in monomer compositions, and protonated aryl ratios. In addition to the main monomers (DHI and DHICA), all the four eumelanins contain quinone methide tautomers. We also find that sepia eumelanin has lower UV absorbance, a smaller ratio of DHICA/DHI and higher protonated aryl carbon ratios than the other three natural eumelanins. Although melanosome morphology differs among the species, they all consist of 10–60 nm subunit nanoparticles. These similarities and differences among different eumelanins from different species will not only help us to understand the changes of their biological functions and chemical structures over the evolutionary history, but also potentially enable us to engineer synthetic eumelanin to achieve enhanced macroscopic properties like UV absorption, photo-protection and radical scavenging.

Data accessibility. All supporting data are either presented in the main text or the electronic supplementary material.

Authors' contributions. The manuscript was written through contributions of all authors. All authors have given approval to the final version of the manuscript.

Competing interests. We declare we have no competing interests.

Funding. This work was supported by the Air Force Office of Scientific Research (FA9550-16-1-0331), National Science Foundation (EAR-1251895 and DMR-1105370), Human Frontier Science Program (RGY-0083) and Japan Society for the Promotion of Science (P16047)

Acknowledgements. We thank Siddhesh Dalvi and Zhorro Nikolov for the help with XPS experiments. We thank Jacob Hill for the help with AFM experiment. We thank Branislav Igic, Bor-Kai Hsiung and Nick Justyn for insightful discussions on the manuscript.

References

1. Zhong J, Frases S, Wang H, Casadevall A, Stark RE. 2008 Following fungal melanin biosynthesis with solid-state NMR: biopolymer molecular structures and possible connections to cell-wall polysaccharides. *Biochemistry* **47**, 4701–4710. (doi:10.1021/bi702093r).
2. Li Q, Clarke JA, Gao K-Q, Zhou C-F, Meng Q, Li D, D'Alba L, Shawkey MD. 2014 Melanosome evolution indicates a key physiological shift within feathered dinosaurs. *Nature* **507**, 350–353. (doi:10.1038/nature12973)
3. Glass K *et al.* 2012 Direct chemical evidence for eumelanin pigment from the jurassic period. *Proc. Natl Acad. Sci. USA* **109**, 10 218–10 223. (doi:10.1073/pnas.1118448109)
4. Hsiung B-K, Blackledge TA, Shawkey MD. 2015 Spiders do have melanin after all. *J. Exp. Biol.* **218**, 3632–3635. (doi:10.1242/jeb.128801)
5. Xiao M, Dhinojwala A, Shawkey M. 2014 Nanostructural basis of rainbow-like iridescence in common Bronzewing *Phaps chalcoptera* feathers. *Opt. Exp.* **22**, 14 625–14 636. (doi:10.1364/OE.22.014625)
6. Simon JD, Peles DN. 2010 The red and the black. *Acc. Chem. Res.* **43**, 1452–1460. (doi:10.1021/ar100079y)
7. Mostert AB, Hanson GR, Sarna T, Gentle IR, Powell BJ, Meredith P. 2013 Hydration-controlled X-band EPR spectroscopy: a tool for unravelling the complexities of the solid-state free radical in eumelanin. *J. Phys. Chem. B* **117**, 4965–4972. (doi:10.1021/jp401615e)
8. Gauden M *et al.* 2008 Role of solvent, pH, and molecular size in excited-state deactivation of key eumelanin building blocks: implications for melanin pigment photostability. *J. Am. Chem. Soc.* **130**, 17 038–17 043. (doi:10.1021/ja806345q)
9. Mostert AB, Powell BJ, Pratt FL, Hanson GR, Sarna T, Gentle IR, Meredith P. 2012 Role of semiconductivity and ion transport in the electrical conduction of melanin. *Proc. Natl Acad. Sci. USA* **109**, 8943–8947. (doi:10.1073/pnas.1119948109)
10. Zhou J, Duan B, Fang Z, Song J, Wang C, Messersmith PB, Duan H. 2014 Interfacial assembly of mussel-inspired Au@Ag@Polydopamine core-shell nanoparticles for recyclable nanocatalysts. *Adv. Mater.* **26**, 701–705. (doi:10.1002/adma.201303032)
11. Li Y *et al.* 2016 Structure and function of iron-loaded synthetic melanin. *ACS Nano* **10**, 10 186–10 194. (doi:10.1021/acsnano.6b05502)
12. Vij M *et al.* 2016 Bioinspired functionalized melanin nanovariants with a range of properties provide effective color matched photoprotection in skin. *Biomacromolecules* **17**, 2912–2919. (doi:10.1021/acs.biomac.6b00740)
13. Liu Y, Ai K, Liu J, Deng M, He Y, Lu L. 2013 Dopamine-melanin colloidal nanospheres: an efficient near-infrared photothermal therapeutic agent for *in vivo* cancer therapy. *Adv. Mater.* **25**, 1353–1359. (doi:10.1002/adma.201204683)
14. Li Y *et al.* 2016 Polycatechol nanoparticle MRI contrast agents. *Small* **12**, 668–677. (doi:10.1002/smll.201502754)
15. Fang C, Deng Y, Xie Y, Su J, Chen G. 2015 Improving the electrochemical performance of Si nanoparticle anode material by synergistic strategies of polydopamine and graphene oxide coatings. *J. Phys. Chem. C* **119**, 1720–1728. (doi:10.1021/jp511179s)
16. Kumar P, Di Mauro E, Zhang S, Pezzella A, Soavi F, Santato C, Cicoira F. 2016 Melanin-based flexible supercapacitors. *J. Mater. Chem. C* **4**, 9516–9525. (doi:10.1039/C6TC03739A)
17. Wang Y, Li T, Wang X, Ma P, Bai H, Dong W, Xie Y, Chen M. 2016 Superior performance of polyurethane based on natural melanin nanoparticles. *Biomacromolecules* **17**, 3782–3789. (doi:10.1021/acs.biomac.6b01298)
18. Panzella L, Melone L, Pezzella A, Rossi B, Pastori N, Perfetti M, D'Errico G, Punta C, d'Ischia M. 2016 Surface-functionalization of nanostructured cellulose aerogels by solid state eumelanin coating. *Biomacromolecules* **17**, 564–571. (doi:10.1021/acs.biomac.5b01497)
19. Bouchoucha M, Tielens F, Gaslain F, CostaTorro F, Casale S, Palcic A, Valtchev V, Lambert J.-F, Jaber M. 2015 Melanin polymerization held in check: a composite of dihydroxyphenylalanine with zeolite beta. *J. Phys. Chem. C* **119**, 8736–8747. (doi:10.1021/acs.jpcc.5b01194)
20. Xiao M, Li Y, Zhao J, Wang Z, Gao M, Gianneschi NC, Dhinojwala A, Shawkey MD. 2016 Stimuli-responsive structurally colored films from bioinspired synthetic melanin nanoparticles. *Chem. Mater.* **28**, 5516–5521. (doi:10.1021/acs.chemmater.6b02127)
21. Wu T-F, Hong J-D. 2015 Dopamine-melanin nanofilms for biomimetic structural coloration. *Biomacromolecules* **16**, 660–666. (doi:10.1021/bm501773c)

22. Xiao M *et al.* 2017 Bioinspired bright noniridescent photonic melanin supraballs. *Sci. Adv.* **3**, e1701151. (doi:10.1126/sciadv.1701151)
23. Shawkey MD, D'Alba L, Xiao M, Schutte M, Buchholz R. 2014 Ontogeny of an iridescent nanostructure composed of hollow melanosomes. *J. Morphol.* **276**, 378–384. (doi:10.1002/jmor.20347)
24. Meredith P, Sarna T. 2006 The physical and chemical properties of eumelanin. *Pigm. Cell Res.* **19**, 572–594. (doi:10.1111/j.1600-0749.2006.00345.x)
25. Watt AA, Bothma JP, Meredith P. 2009 The supramolecular structure of melanin. *Soft Matter* **5**, 3754–3760. (doi:10.1039/b902507c)
26. Cheng J, Moss SC, Eisner M, Zschack P. 1994 X-Ray characterization of melanins-I. *Pigm. Cell Res.* **7**, 255–262. (doi:10.1111/j.1600-0749.1994.tb00060.x)
27. d'Ischia M *et al.* 2013 Melanins and melanogenesis: methods, standards, protocols. *Pigm. Cell Melanoma Res.* **26**, 616–633. (doi:10.1111/pcmr.12121)
28. Dreyer DR, Miller DJ, Freeman BD, Paul DR, Bielawski CW. 2012 Elucidating the structure of poly(dopamine). *Langmuir* **28**, 6428–6435. (doi:10.1021/la204831b)
29. Ding Y, Weng L-T, Yang M, Yang Z, Lu X, Huang N, Leng Y. 2014 Insights into the aggregation/deposition and structure of a polydopamine film. *Langmuir* **30**, 12 258–12 269. (doi:10.1021/la5026608)
30. Li Y, Liu J, Wang Y, Chan HW, Wang L, Chan W. 2015 Mass spectrometric and spectrophotometric analyses reveal an alternative structure and a new formation mechanism for melanin. *Anal. Chem.* **87**, 7958–7963. (doi:10.1021/acs.analchem.5b01837)
31. Liebscher J, Mrówczyński R, Scheidt HA, Filip C, Hădade ND, Turcu R, Bende A, Beck S. 2013 Structure of polydopamine: a never-ending story? *Langmuir* **29**, 10 539–10 548. (doi:10.1021/la4020288)
32. Chatterjee S, Prados-Rosales R, Tan S, Itin B, Casadevall A, Stark RE. 2014 Demonstration of a common indole-based aromatic core in natural and synthetic eumelanins by solid-state NMR. *Org. Biomol. Chem.* **12**, 6730–6736. (doi:10.1039/C4OB01066C)
33. Tuna D, Udvarhelyi A, Sobolewski AL, Domcke W, Domratcheva T. 2016 Onset of the electronic absorption spectra of isolated and π-stacked oligomers of 5,6-dihydroxyindole: an ab initio study of the building blocks of eumelanin. *J. Phys. Chem. B* **120**, 3493–3502. (doi:10.1021/acs.jpcb.6b01793)
34. Chen C-T, Ball V, de Almeida Gracio JJ, Singh MK, Toniazzo V, Ruch D, Buehler MJ. 2013 Self-assembly of tetramers of 5,6-dihydroxyindole explains the primary physical properties of eumelanin: experiment, simulation, and design. *ACS Nano* **7**, 1524–1532. (doi:10.1021/nn305305d)
35. Kaxiras E, Tsolakidis A, Zonios G, Meng S. 2006 Structural model of eumelanin. *Phys. Rev. Lett.* **97**, 218102. (doi:10.1103/PhysRevLett.97.218102)
36. Chen CT, Chuang C, Cao J, Ball V, Ruch D, Buehler MJ. 2014 Excitonic effects from geometric order and disorder explain broadband optical absorption in eumelanin. *Nat. Commun.* **5**, 3859. (doi:10.1038/ncomms4859)
37. Bernsmann F, Ball V, Addiego F, Ponche A, Michel M, Gracio JJA, Toniazzo V, Ruch D. 2011 Dopamine-melanin film deposition depends on the used oxidant and buffer solution. *Langmuir* **27**, 2819–2825. (doi:10.1021/la104981s)
38. Kim HW, McCloskey BD, Choi TH, Lee C, Kim M-J, Freeman BD, Park HB. 2013 Oxygen concentration control of dopamine-induced high uniformity surface coating chemistry. *ACS Appl. Mater. Interfaces* **5**, 233–238. (doi:10.1021/am302439g)
39. Corani A, Huijser A, Gustavsson T, Markovitsi D, Malmqvist PA, Pezzella A, d'Ischia M, Sundstrom V. 2014 Superior photoprotective motifs and mechanisms in eumelanins uncovered. *J. Am. Chem. Soc.* **136**, 11 626–11 635. (doi:10.1021/ja501499q)
40. Bernsmann F, Ponche A, Ringwald C, Hemmerlé, J., Raya J, Bechinger B, Voegel J-C, Schaaf P, Ball V. 2009 Characterization of dopamine-melanin growth on silicon oxide. *J. Phys. Chem. C* **113**, 8234–8242. (doi:10.1021/jp901188h)
41. Clark MB, Gardella JA, Schultz TM, Patil DG, Salvati L. 1990 Solid-state analysis of eumelanin biopolymers by electron spectroscopy for chemical analysis. *Anal. Chem.* **62**, 949–956. (doi:10.1021/ac00208a011)
42. Liu Y, Hong L, Wakamatsu K, Ito S, Adhyaru B, Cheng CY, Bowers CR, Simon JD. 2005 Comparison of structural and chemical properties of black and red human hair melanosomes. *Photochem. Photobiol.* **81**, 135–144. (doi:10.1034/j.1600-0749.2003.00059.x)
43. Tian S, Garcia-Rivera J, Yan B, Casadevall A, Stark RE. 2003 Unlocking the molecular structure of fungal melanin using 13c biosynthetic labeling and solid-state NMR. *Biochemistry* **42**, 8105–8109. (doi:10.1021/bi0341859)
44. Katritzky AR, Akhmedov NG, Denisenko SN, Denisko OV. 2002 ^{1}H NMR spectroscopic characterization of solutions of sepia melanin, sepia melanin free acid and human hair melanin. *Pigm. Cell Res.* **15**, 93–97. (doi:10.1034/j.1600-0749.2002.1o062.x)
45. Liu Y, Kempf VR, Brian Nofsinger J, Weinert EE, Rudnicki M, Wakamatsu K, Ito S, Simon JD. 2003 Comparison of the structural and physical properties of human hair eumelanin following enzymatic or acid/base extraction. *Pigm. Cell Res.* **16**, 355–365. (doi:10.1034/j.1600-0749.2003.00059.x)
46. Xiao M, Li Y, Allen MC, Deheyn DD, Yue X, Zhao J, Gianneschi NC, Shawkey MD, Dhinojwala A. 2015 Bio-inspired structural colors produced *via* self-assembly of synthetic melanin nanoparticles. *ACS Nano* **9**, 5454–5460. (doi:10.1021/acsnano.5b01298)
47. Mao J, Hu W, Schmidt-Rohr K, Davies G, Ghabbour E, Xing B. 2000 Quantitative characterization of humic substances by solid-state carbon-13 nuclear magnetic resonance. *Soil Sci. Soc. Am. J.* **64**, 873–884. (doi:10.2136/sssaj2000.643873x)
48. Mao J-D, Schmidt-Rohr K. 2004 Accurate quantification of aromaticity and nonprotonated aromatic carbon fraction in natural organic matter by ^{13}C solid-state nuclear magnetic resonance. *Environ. Sci. Technol.* **38**, 2680–2684. (doi:10.1021/es034770x)
49. Sommer W, Gottwald J, Demco D, Spiess HW. 1995 Dipolar heteronuclear multiple-quantum NMR spectroscopy in rotating solids. *J. Magn. Reson. Ser A* **113**, 131–134. (doi:10.1006/jmra.1995.1068)
50. Hellström AR *et al.* 2011 Inactivation of Pmel alters melanosome shape but has only a subtle effect on visible pigmentation. *PLoS Genet.* **7**, e1002285. (doi:10.1371/journal.pgen.1002285)
51. Liu Y, Simon JD. 2003 Isolation and biophysical studies of natural eumelanins: applications of imaging technologies and ultrafast spectroscopy. *Pigm. Cell Melanoma Res.* **16**, 606–618. (doi:10.1046/j.1600-0749.2003.00098.x)
52. Ito S, Wakamatsu K. 2008 Chemistry of mixed melanogenesis-pivotal roles of dopaquinone. *Photochem. Photobiol.* **84**, 582–592. (doi:10.1111/j.1751-1097.2007.00238.x)
53. Panzella L, Gentile G, D'Errico G, Della Vecchia NF, Errico ME, Napolitano A, Carfagna C, d'Ischia M. 2013 Atypical structural and pi-electron features of a melanin polymer that lead to superior free-radical-scavenging properties. *Angew. Chem. Int. Ed.* **52**, 12 684–12 687. (doi:10.1002/anie.201305747)
54. Malitson I. 1965 Interspecimen comparison of the refractive index of fused silica. *J. Opt. Soc. Am.* **55**, 1205–1208. (doi:10.1364/JOSA.55.001205)
55. Zangmeister RA, Morris TA, Tarlov MJ. 2013 Characterization of polydopamine thin films deposited at short times by autoxidation of dopamine. *Langmuir* **29**, 8619–8628. (doi:10.1021/la400587j)
56. Centeno SA, Shamir J. 2008 Surface Enhanced Raman Scattering (SERS) and FTIR characterization of the sepia melanin pigment used in works of art. *J. Mol. Struct.* **873**, 149–159. (doi:10.1016/j.molstruc.2007.03.026)
57. Adhyaru BB, Akhmedov NG, Katritzky AR, Bowers CR. 2003 Solid-state cross-polarization magic angle spinning ^{13}C and ^{15}N NMR characterization of sepia melanin, sepia melanin free acid and human hair melanin in comparison with several model compounds. *Magn. Reson. Chem.* **41**, 466–474. (doi:10.1002/mrc.1193)
58. Thureau P, Ziarelli F, Thévand A, Martin RW, Farmer PJ, Viel S, Mollica G. 2012 Probing the motional behavior of eumelanin and pheomelanin with solid-state NMR spectroscopy: new insights into the pigment properties. *Chem. Eur. J.* **18**, 10 689–10 700. (doi:10.1002/chem.201200277)
59. Thakur KA, Kean RT, Zupfer JM, Buehler NU, Doscotch MA, Munson EJ. 1996 Solid state ^{13}C CP-MAS NMR studies of the crystallinity and morphology of poly (L-lactide). *Macromolecules* **29**, 8844–8851. (doi:10.1021/ma960828z)
60. Brown SP. 2007 Probing proton-proton proximities in the solid state. *Prog. Nucl. Magn. Reson. Spectrosc.* **50**, 199–251. (doi:10.1021/ja045461p)
61. Lee M, Kim J-W, Peleshanko S, Larson K, Yoo Y-S, Vaknin D, Markutsya S, Tsukruk VV. 2002 Amphiphilic

Hairy disks with branched hydrophilic tails and a hexa-*p*-eri-hexabenzocoronene core. *J. Am. Chem. Soc.* **124**, 9121–9128. (doi:10.1021/ja017553+)

62. Hansen M, Feng X, Macho V, Müllen K, Spiess HW, Floudas G. 2011 Fast and slow dynamics in a discotic liquid crystal with regions of columnar order and disorder. *Phys. Rev. Lett.* **107**, 257801. (doi:10.1103/PhysRevLett.107.257801)
63. Yang C, Hu JG, Heeger AJ. 2006 Molecular structure and dynamics at the interfaces within bulk heterojunction materials for solar cells. *J. Am. Chem. Soc.* **128**, 12 007–12 013. (doi:10.1021/ja063707f)
64. Luo Y-R. 2002 *Handbook of bond dissociation energies in organic compounds*. Boca Raton, FL: CRC press.
65. Duer MJ. 2008 *Solid state NMR spectroscopy: principles and applications*. New York, NY: John Wiley & Sons.
66. Il'ichev YV, Simon JD. 2003 Building blocks of eumelanin: relative stability and excitation energies of tautomers of 5,6-dihydroxyindole and 5,6-indolequinone. *J. Phys. Chem. B* **107**, 7162–7171. (doi:10.1021/jp034702x)